RETRACTED: Assessment of the Effect of Transition Metal Oxide Addition on the Conductivity of Commercial Gd-Doped Ceria

Kerstin Neuhaus,[1,*,z] Raimund Dolle,[2] and Hans-Dieter Wiemhöfer[1,2]

[1]*Institute of Inorganic and Analytical Chemistry, University of Münster, 48149 Münster, Germany*
[2]*Forschungszentrum Jülich GmbH, Institute of Energy and Climate Research, Helmholtz-Institute Münster: Ionics in Energy Storage (IEK-12), 48149 Münster, Germany*

The effect of addition of transition metal oxides on the charge transport of commercially available Gd-doped ceria ($Ce_{0.9}Gd_{0.1}O_{2-\delta}$) was assessed with special emphasis on the electronic partial conductivity. The samples were doped by adding 2, 4 or 6 cat% of $CoO_{3/4}$ or $FeO_{2/3}$, or 2 mol% of the transition metal oxides V_2O_5, MnO_2, and CuO, respectively. It was found that even small amounts of transition metal oxides severely change the partial electronic conductivity of ceria while the majority oxygen ion conductivity was only mildly affected: for high oxygen ion conductivity, Fe or Mn oxide addition as well as small amounts of Co oxide are beneficial, as especially the grain boundary conductivity is slightly increased. Addition of V or Cu oxide in contrast increases the minority charge carrier conductivity of electrons and thus enhances the mixed ionic-electronic conductivity. For Co oxide addition, an increasing electronic conductivity with decreasing oxygen partial pressure from 10^{-8} to 10^{-4} bar at temperatures below 600°C indicates the changing redox state of Co from divalent at low oxygen partial pressures to trivalent under ambient oxygen partial pressure.

 [DOI: 10.1149/2.1111807jes]

Manuscript submitted March 15, 2018; revised manuscript received May 3, 2018. Published May 18, 2018.

Composites of acceptor doped ceria and good electron conductors like certain transition metal containing perovskites or spinels have come into focus during the last years for usage in fuel-cell electrodes or for catalyst applications.[1–5] It has been observed that during co-sintering of ceria and various transition metal oxides, part of the metal oxide dissolves with interdiffusion of the additional cations between both phases.[6–8] This may lead to a less defined trace metal concentration in the main ceria phase. A similar mechanism can take place, if ceria is in contact to metal interconnects e.g. in an SOFC cell stack at high temperatures.[9] Apart from unintended transition metal cation doping, deliberate introduction of various metal cations into a ceria host matrix has shown promising effects for catalytic applications of ceria.[10–15]

It has been shown by a vast amount of publications that the addition of substituent cations from added metal oxides into a ceria matrix can have various different effects on the partial electronic or oxygen ion conductivity apart from higher valent cations reacting solely as a donor (e.g. Ta, Nb, W)[16–18] or - as in most cases - as acceptor dopant (e.g. Gd, Sm, Y, Ca, Nd etc.):[19–22] Some oxides such as Pr_2O_3 or MnO_2 have been found to add an additional electronic state in the ceria bandgap and therefore to significantly increase the electronic conductivity.[23,24] Pr as a redox active material also provides an additional oxygen partial pressure dependent maximum of the electronic conductivity due to the reduction from Pr^{4+} to Pr^{3+} and a related polaron hopping mechanism within a certain oxygen partial pressure range.[23,25,26] A comparable effect has also been confirmed for Mn doping in YSZ or ceria after sintering at certain temperatures to preserve the Mn^{3+} state within the material[27–29] and is also conceivable for other redox-active transition metal cations.

Apart from the effect by substitution of the cerium cation, the segregation of small amounts of dopants or immiscible additives at the grain boundaries can severely influence pathways of the electron or oxygen ion transport within the material. Avila-Paredes et al. and other groups found out that the introduction of small amounts of Fe, Co, Mn, or Cu to Gd-doped ceria results in significant reduction of the grain boundary resistivity of the samples[30–33] while the total conductivity remains nearly similar or is even reduced in case of Mn.[33,34]

Especially Co[32,35,36] and Fe,[32,36–38] but to a lesser extent also Mn,[28,38,39] Ni,[36,38] Cu[32,38] and Zn[40,41] have besides been reported to facilitate the sintering of ceria ceramics while Cr, in contrast, was observed to suppress the sinterability of ceria.[31,35] At the same time, all transition metals, which were improving the sintering process were found to modify the charge transport within acceptor doped ceria as well.[25,31,36] Zn, for instance improves the sinterability and works as an acceptor dopant in ceria.[40] For doping with Co, a significantly increased electronic transport has been found by several groups[25,31,32,42,43] and similar observations have been reported for Fe, Cu, and Mn addition.[24,29,32]

The effect was mainly attributed to exclusive segregation of the transition metals into the grain boundary core, where they are thought to either form separate highly electron conducting phases[42–45] or to decrease the grain boundary surface charge by variation of the local defect concentrations leading to a lower grain boundary resistivity of the majority charge carriers.[30,46] In case of Mn, simulations and measurements showed that the increased electronic partial conductivity with increasing Mn addition can be attributed to an additional Mn 3d-related state between the top of the valence band and the bottom of the Ce 4f band.[24,29] Also Khare et al. observed the development of an additional feature at the binding energy position of 2.6 eV in the valence band of CeO_2 after doping with 2–6 mol% iron.[47] This feature is related to the introduction of an additional Fe-d level which can work as a "stepping stone" for electrons within the broad ceria bandgap.

Apart from the ions listed above, V could also be of interest for interdiffusion into ceria, as V_2O_5 is a widely used catalyst additive and the catalytic activity of ceria-V_2O_5 mixtures or V_2O_5 on ceria supports has already been a focus of research.[12,48] It has been found that the addition of V_2O_5 to La-doped ceria increases the sinterability of the material but decreases the total conductivity.[49] This could be an indication for a possible donor doping nature of the V^{5+} cation, as donor and acceptor doping in ceria counteract each other.[16] Nb^{5+} and Ta^{5+} already have been found to act as donor dopants in ceria,[16–18] therefore a donor doping effect of V^{5+} is possible, but a detailed study concerning the effect of V^{5+} substitution on the conductivity of ceria is missing so far.

The effect of small amounts of various transition metal oxides on the electronic partial conductivity has already been investigated previously in detail by us for Cr,[31] Co,[25] Mn[24] and Zn addition.[40] A detailed comparative study of the effect of transition metal addition on the electronic conductivity over a large temperature and oxygen partial pressure range deploying a commercially available model material has not been performed to date, though.

For all transition metals, the solubility in the ceria host matrix is relatively low, although the range of proposed soluble concentration between different studies for the respective cations is considerable

*Electrochemical Society Member.
[z]E-mail: kerstin.neuhaus@uni-muenster.de

Table I. Composition, purity and manufacturer of educts.

Composition	Purity	Manufacturer
$Ce_{0.9}Gd_{0.1}O_{1.95}$	99.99%	Aldrich
V_2O_5	99.99%	Aldrich
MnO_2	99%	Acros Organics
Fe_2O_3	98%	Riedel-de Haën
Co_3O_4	99%	ChemPur
CuO	99.999%	abcr

(e.g. varying from 56 mol%[50] to 0.6 mol%[51] for Zn or between 5–10 mol%[52] to < 1 mol% for Mn[34] in ceria). Obviously, the amount of incorporated metal cations as well as their valence in sintered ceria depends strongly on the preparation method, sintering temperature and co-dopant concentrations[28,32,33] which underlines the importance of an investigation of charge carrier transport for materials with a standardized (commercial) ceria host matrix.

In the investigation presented here, the effect of adding V_2O_5, MnO_2, Fe_2O_3, Co_3O_4, and CuO on the charge transport characteristics and especially on the electronic partial conductivity of commercially available 10 mol% Gd-doped ceria was assessed. As Fe and Co containing perovskites or spinels are the most commonly investigated compounds when preparing oxide composites with ceria, a special emphasis was put on Fe_2O_3 and Co_3O_4 addition. Therefore, CGO samples with 2, 4 and 6 cat% Fe or Co addition were prepared for easier comparison with existing literature, while for the other transition metals, 2 mol% of the respective oxide was added.

Experimental

Sample preparation.—The samples were prepared from commercially available $Ce_{0.9}Gd_{0.1}O_{2-\delta}$ powder (Sigma-Aldrich) in combination with the respective metal oxides. Composition, purity and manufacturer of the educts are listed in Table I.

The powders were milled for 3 h in ethanol in a planetary ball mill. After drying for 24 h at 70°C, the powders were pressed into pellets and afterwards sintered in air.

The pristine CGO sample was sintered at 1600°C for 8 h, all other samples were sintered at 1300°C for 4 h. This temperature was chosen, because several studies suggested, that Fe is not soluble in ceria below temperatures of 1200°C and that optimal densification is received at 1300°C.[53–55] In order to keep the parameters similar for all samples, 1300°C was chosen as a sintering temperature for all transition metal containing samples. No individual optimization of sintering temperatures was performed.

After sintering, all samples were investigated for impurities using XRD. Additionally, the density was measured by SEM imaging and Archimedean weighing. All received samples were relatively dense with a low amount of pinholes. The average grain sizes were calculated from SEM images using the lineal intercept method.[56] The respective sintering parameters, the received densities, as well as the average grain sizes and abbreviations for the sample compositions are listed in Table II.

Impedance spectroscopy.—Impedance measurements in air were carried out as a function of temperature in ambient air using a Novotherm HT 1200 oven with an Alpha-A frequency analysator (NovoControl GmbH). Pt resinate paste (RP 070107, Heraeus GmbH) was applied directly on the sample pellets and was sintered at 850°C before measurement to minimize any contact resistance. The paste electrodes were contacted by a Pt-sheet. An AC peak-to-peak amplitude of 40 mV was chosen. All measurements were carried out in ambient air and in a temperature range from 200–800°C. All measurements were executed in a heating and in a cooling cycle, respectively, to check possible deterioration of the samples.

The experimental frequency dependence of the impedance was fitted using the software package ZView 2 (Scribner Associates, Inc.) with regard to the medium and high frequency range. For fitting, an equivalent circuit with two resistors in series, which each have a constant phase element (CPE) in parallel, was used (cf. Fig. 1).[57] One resistor/constant phase element can be assigned to bulk characteristics (R2/CPE1) and one to effective grain boundary characteristics (R3/CPE2), respectively. The resistivity of the sample-electrode interface was also included as a single resistor in series (R1), but the resistivity of the interface was negligible in comparison to the resistivity of the samples (1–1000 Ohms depending on the temperature). The ideality parameter of the constant phase element in the equivalent circuits which is between 0 (perfect inductance) and 1 (perfect capacitor) typically varied between 0.4 and 1 depending on sample composition and temperature.

Bulk (σ_b) and effective grain boundary conductivities (σ_{gb}) have the following definition within the brick layer model:

$$R_{total} = R_b + R_{gb} = \frac{n}{A} \cdot \left(\frac{1}{\sigma_b} \cdot L_g + \frac{1}{\sigma_{gb}} \cdot L_{gb} \right) = \frac{1}{\sigma_t} \quad [1]$$

Here, n is the number of grains along the sample between the contacts, A is the surface area at the contacts, L_g is the average grain length (cf. Table II), L_{gb} is the average thickness of the grain boundary which was in our case assumed to be 1 nm.[58,59] The effective grain boundary conductivity was corrected with the factor $\frac{L_{gb}}{L_g}$ according to the brick layer model.

As it is recommended to use the ratio of bulk and grain boundary capacitance for correction of the grain boundary conductivity,[60,61] we also tried this way of evaluation (see σ_{gb}^{**} in example in Fig. 2), as the grain boundary thickness in our case is only an estimate. Compared to the values derived using grain size and grain boundary thickness, the grain boundary conductivity σ_{gb}^{**} calculated using the capacitances showed a much poorer Arrhenius behavior for all samples (cf. Fig. 2) with a comparably good accordance only in the intermediate temperature regime. In the high temperature regime, the capacitances were not analyzable in some cases due to poor separation of the

Table II. Sintering parameters, received densities in percent of the theoretical density calculated from XRD measurements, average grain sizes, and lattice constants (*a*) for the respective samples. The compositions are the nominal compositions of the samples, which were received for the green bodies. A slight transition metal loss during sintering is probable.

Composition	Sintering parameters	Density	Av. grain size/µm	*a*/Å	Abbr.
$Ce_{0.9}Gd_{0.1}O_{1.95}$	1600°C, 8 h	96.3%	1.98 ± 0.97	5.42(9)	CGO
$V_{0.04}Ce_{0.9}Gd_{0.1}O_{2-\delta}$	1300°C, 8 h	99.0%	0.76 ± 0.21	5.41(6)	CGOV4
$Mn_{0.02}Ce_{0.9}Gd_{0.1}O_{2-\delta}$	1300°C, 4 h	99.5%	1.37 ± 0.54	5.42(9)	CGOMn2
$Fe_{0.06}Ce_{0.9}Gd_{0.1}O_{2-\delta}$	1300°C, 4 h	97.8%	0.88 ± 0.43	5.42(1)	CGOFe6
$Fe_{0.04}Ce_{0.9}Gd_{0.1}O_{2-\delta}$	1300°C, 4 h	98.5%	1.05 ± 0.37	5.41(3)	CGOFe4
$Fe_{0.02}Ce_{0.9}Gd_{0.1}O_{2-\delta}$	1300°C, 4 h	98.8%	0.92 ± 0.34	5.43(7)	CGOFe2
$Co_{0.06}Ce_{0.9}Gd_{0.1}O_{2-\delta}$	1300°C, 4 h	99.6%	1.32 ± 0.36	5.43(3)	CGOCo6
$Co_{0.04}Ce_{0.9}Gd_{0.1}O_{2-\delta}$	1300°C, 4 h	98.0%	1.12 ± 0.45	5.43(3)	CGOCo4
$Co_{0.02}Ce_{0.9}Gd_{0.1}O_{2-\delta}$	1300°C, 4 h	99.4%	1.18 ± 0.55	5.43(7)	CGOCo2
$Cu_{0.02}Ce_{0.9}Gd_{0.1}O_{2-\delta}$	1300°C, 4 h	97.9%	1.60 ± 0.75	5.43(3)	CGOCu2

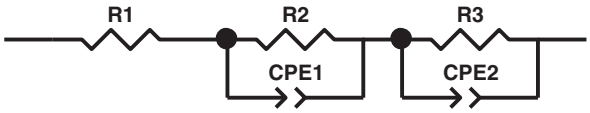

Figure 1. Equivalent circuit used for evaluation of impedance spectroscopy measurements.

bulk and grain boundary arc contributions in the impedance spectroscopy data, and the capacitances from lower temperatures additionally deformed the plot. Therefore, we decided to use σ^{*}_{gb} for further evaluation.[58,62]

Activation energies were calculated from Arrhenius diagrams of the respective conductivities.

Microcontact Hebb-Wagner measurements.—The electronic partial conductivity of the samples was investigated using a modified Hebb-Wagner setup. In this experimental setup an encapsulated platinum microcontact is applied as working electrode and a Pt sheet as counter electrode. The sample was fixed to the Pt sheet with Pt resinate paste (RP 070107, Heraeus GmbH). An extended description of the microcontact measurement method can be found in previous publications.[24,63–65]

Measurements were executed at temperatures between 800–400°C. Polarization of the samples was preformed from 0 to −0.8 V and back again. Additionally, randomly selected sample compositions were measured several times to prove reproducibility. The presented values are average values with error bars showing the standard deviations. All electron conductivity values were corrected for the microcontact diameter, which was determined by measuring the contact print in the glass encapsulation using light microscopy after detaching the microcontact at the finish of the measurement. Contact radii were in the range 150–400 μm.

Results and Discussion

Microstructure and density.—All prepared samples were found to be phase pure in XRD measurements (cf. Fig. 3). It can be seen from Table II that for the pure CGO material, which was produced with a higher sintering temperature, the largest average grain sizes were received (also see Fig. 4). Although the sintering temperatures and times were lower for all the transition metal-doped samples, all samples showed higher densities than the pristine CGO sample, which is in good accordance to the well-investigated improvement of sinter-

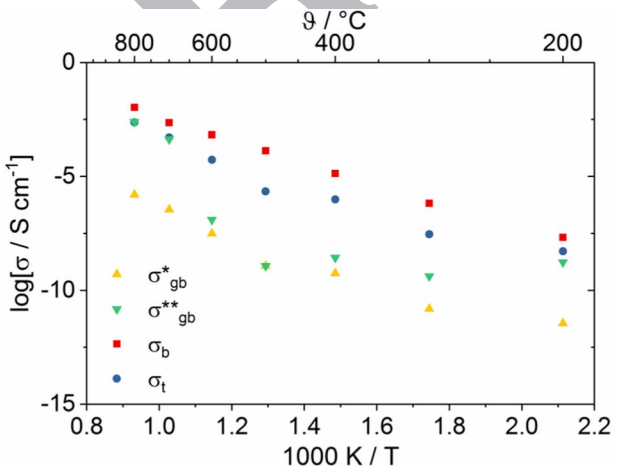

Figure 2. Bulk and total conductivity as well as effective grain boundary conductivity evaluated from using the ratio of grain boundary thickness and grain size (σ^{*}_{gb}) and using the ratio of bulk and grain boundary capacity (σ^{**}_{gb}) for pure CGO10.

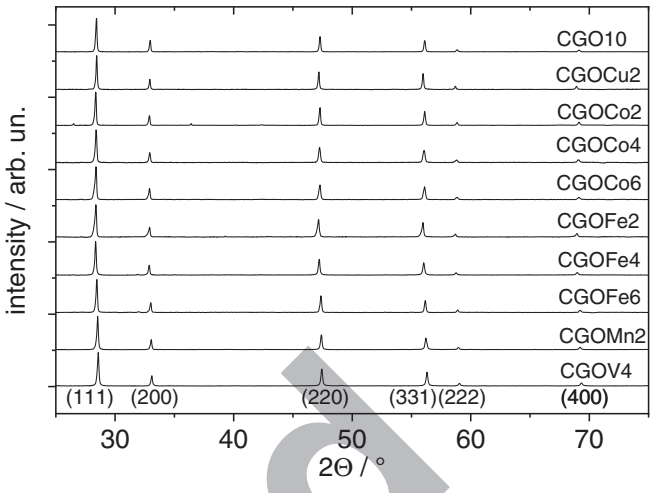

Figure 3. X-ray diffractograms of the respective samples. All samples were single phase fluorite material within the detection limits of XRD.

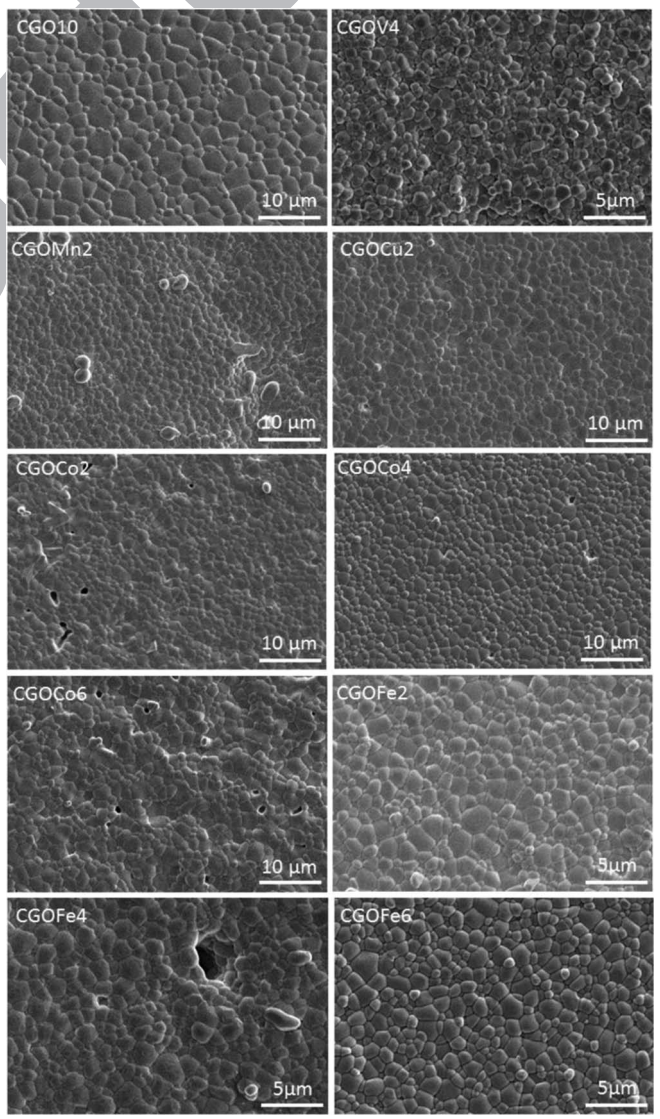

Figure 4. SEM images of the samples. Note the different resolutions of the images.

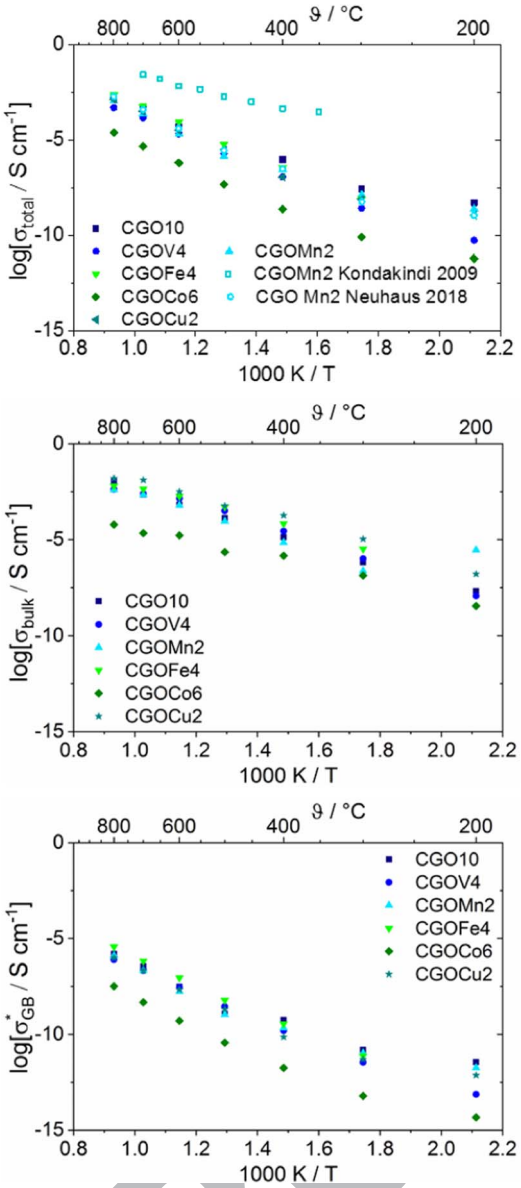

Figure 5. Bulk, grain boundary and total conductivities for the samples with 2 mol% oxide addition. For Fe addition, the results at 200°C were not evaluable. Additional results for the total conductivity of CGOMn2 from literature Refs. 53 and 24 are shown as open symbols in the uppermost graph.

ability of Co, Fe, Mn and Cu. In accordance to the findings of Fagg et al. a decrease of the average grain size of the Fe, Co and Cu doped materials was found in the sequence Cu > Co > Fe.[32]

V addition also led to very dense samples, which is in good accordance to previous findings,[49] but the grain size was considerably lower for CGOV4 compared to all other compositions.

It is not clear, which valence was adopted by the cations during sintering. In case of Mn, previous publications suggest the incorporation as Mn^{2+} at the chosen sintering temperature in air.[27–29] Fe can be assumed to exist mostly in the trivalent state (except at very low oxygen partial pressures). For Co, previous studies suggested the incorporation of divalent Co,[25] but incorporation as a trivalent species would also be possible. The valence of V and Cu when dissolved in ceria remains unclear up to now.

Impedance spectroscopy.—From impedance spectroscopy of the five different samples with 2 mol% oxide addition (depicted in Fig. 5) only minor effects are seen for the total conductivity: a slight increase of the total conductivity in the high temperature range referring to the pristine material was found for iron, cobalt and copper doped samples.

The addition of V leads to a minor decrease of the electrical conductivity compared to pristine CGO, especially in the low temperature range between 200–400°C. This could either be interpreted as a hint that V works as a donor dopant in ceria, as the effects of donor and acceptor doping counteract to each other,[16] therefore the oxygen ion conductivity - which is the majority charge carrier in CGO - should decrease in acceptor doped ceria after a slight donor dopant addition. The other possibility is that V works in a similar way to Cr and inhibits grain growth (cf. Table II) as well as lowers the overall transport performance of the material.

For CGOCo2 to CGOCo4, and CGOFe2 to CGOFe6, the bulk and grain boundary conductivities are slightly enhanced in comparison to pure CGO. The concentration increase does not have a pronounced effect on the electrical conductivity (cf. Fig. 6) in case of Fe, but in case of Co, a decrease of the grain and grain boundary conductivity and also of the total conductivity for CGOCo6 are observed. In comparison to literature values from Ref. 31 (CGOCo2) and Ref. 53 (CGOFe2), the measured values from our study are lower by about two decades. For both studies, the transition metals were added to CGO powder as solution of the respective nitrates in ethanol, as was done in several other studies concerning transition metal addition to ceria.[32,53,54] Apparently, this leads to a better distribution of the transition metals and optimizes the initial increase of grain boundary conductivity.

The influence of the grain boundary conductivity of all samples was evaluated by calculating the blocking factor α_{gb} which is defined as the ratio of the effective grain boundary resistance divided by the total resistance:[38,66]

$$\alpha_{gb} = \frac{R_{gb}}{(R_{bulk} + R_{gb})} \quad [2]$$

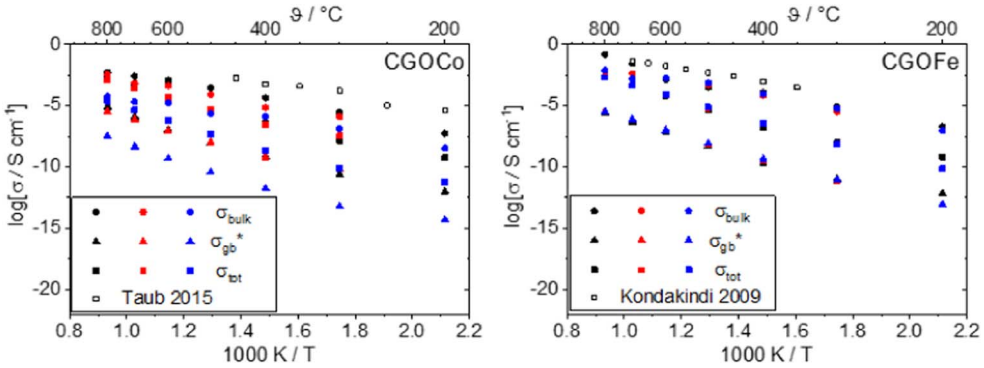

Figure 6. Bulk, grain boundary and total conductivities for the Co and Fe containing samples. Black symbols are for 2 cat%, red symbols for 4 cat%, and blue symbols for 6 cat% Co or Fe addition, respectively. Open symbols show total conductivity of $Co_{0.02}Ce_{0.9}Gd_{0.1}O_2$[31] and $Fe_{0.02}Ce_{0.9}Gd_{0.1}O_2$.[53]

Table III. Blocking factor α_{gb} for all samples at chosen temperatures. The experimental error is in the range of 5%.

Composition	α_{gb} 500°C	600°C	700°C
CGO	0.92	0.81	0.76
CGOV4	0.99	0.98	0.94
CGOMn2	0.98	0.96	0.89
CGOFe6	0.99	0.96	0.70
CGOFe4	0.99	0.95	0.86
CGOFe2	0.99	0.95	0.98
CGOCo6	0.98	0.96	0.78
CGOCo4	0.63	0.51	0.26
CGOCo2	0.98	0.95	0.79
CGOCu2	0.99	0.99	0.97

This factor gives the fraction of charge carriers which are partially blocked at impenetrable internal interfaces with respect to the total sum of electric charge carriers.[38] The values for α_{gb} for all samples at chosen temperatures can be found in Table III. As at least at high temperatures in most of cases considered here – apart from CGOCo6 – we found $\sigma_{O^{2-}} >> \sigma_e$, and the ion transport is partially blocked by the grain boundaries, the blocking factor gives us a good idea about the degree of blockade of the grain boundaries for oxygen ion transport. At the same time, grain boundaries can still be pathways for good electronic conduction.

Small grains and grain boundaries of acceptor doped ceria are commonly described by a space charge model, where the grain surface carries a surface charge with the compensating countercharge in the space charge region below the surface. This describes the grain boundaries in terms of a Mott-Schottky type contact.[67] The space charge potential difference between the surface and the bulk potential denoted by $\Delta\varphi_{GB}$ is defined by

$$\Delta\varphi_{GB} = \varphi_{GB} - \varphi_{bulk} \quad [3]$$

The existence of the space charge potential difference is accompanied by a defect concentration gradient between the bulk and the grain boundary along the space charge domain.[30,46,68,69] Together with the most often found positive surface charge at the grain boundary core in acceptor doped ceria,[46] there is a depletion of positive oxygen vacancies in the near surface range. This effectively slows down the transfer of vacancies and hence of oxygen ions between two grains perpendicular to the grain boundaries. On the other hand, electron transport through the grain boundary core as well as along the adjacent space charge layer is favored.

The potential barrier height $\Delta\varphi_{GB}$ between the grain boundary and the bulk grain can be calculated using the bulk and grain boundary resistances from impedance spectroscopy by solving the following equation numerically and plotting the intercept between the linear and the exponential term at $x > 0.02$:[67]

$$\frac{\rho_{gb}}{\rho_{bulk}} = \exp\left(\frac{2e\Delta\varphi_{GB}}{kT}\right) \cdot \frac{kT}{4e\Delta\varphi_{GB}} \quad [4]$$

Here, ρ_{gb} is the grain boundary resistivity, ρ_{bulk} is the bulk resistivity, e is the elementary charge, k is the Boltzmann constant in J/K, and T is the absolute temperature in K.[30]

The space charge potential barrier is heavily dependent on grain size[70] and dopant allocation and concentration.[71] This makes comparison of absolute values to other samples difficult, even if they have the same composition. Trends for the different materials should nevertheless be the same, therefore it can be used as a sensitive indicator for changes of the defect chemistry at the grain boundaries.

The potential barrier height for the different samples is shown in Fig. 7 as a function of temperature. It can be seen, that for all compositions the potential barrier height is increased with respect to the pristine CGO10, except at temperatures of 700°C or higher. Apart from CGOFe2, all samples follow a more or less similar trend where the potential barrier height decreases with increasing temperature. For CGOFe2, this is not the case: here, the highest $\Delta\varphi_{GB}$ of all tested

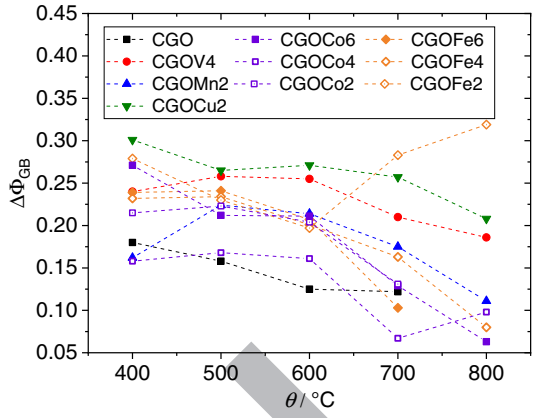

Figure 7. Grain boundary potential barrier for all samples in the temperature range between 400–800°C. The error is estimated to be in the area of 0.05 V. The differences between grain and grain boundary resistances for the pristine CGO10, CGOCo2, and CGOFe6 were so low at 800°C, that Eq. 4 could not be solved anymore.

samples can be found at 700–800°C, while in the temperature range between 600–400°C, the values are quite similar to the rest of the samples. Apart from CGOFe2, CGOCu2 shows the highest values for the potential barrier throughout the whole temperature range.

From comparison of the blocking factor and the grain boundary potential barrier, we can deduce that in all cases the addition of transition metal oxides leads to a more pronounced oxygen ion transport blocking of the grain boundaries. This in good accordance to the widely accepted findings, that transition metal cations only have a low solubility in ceria and mainly segregate at the grain boundaries.[30,32,42–44] In case of Co and Fe addition, a significantly lower blocking effect in the low temperature regime can be observed for addition of higher amounts of Co or Fe, respectively. Optimal results were received for CGOCo4, where the blockage of the grain boundaries is comparably low at all investigated temperatures. For all other compositions, the blocking effect is still somewhat higher than in pure CGO.

The Arrhenius plot of the conductivities was also deployed to calculate activation energies for bulk and grain boundary transport. From Table IV it can be observed, that the activation energies for the total conductivity are increased by addition of transition metal oxides in comparison to the pristine CGO. The most severe increase was found for Fe and Co addition. The increase of the activation energies of the total conductivity (being practically equal to the oxygen ion conduction) can be attributed to strongly increased grain boundary activation energies $E_{A,gb}$. At the same time, a small reduction of the $E_{A,bulk}$ was measured for samples with 2 cat% Cu and 2 cat% Co addition. 6 cat% Co addition led to a severe decrease of the activation energy for bulk transport.

For the six investigated samples with Co and Fe addition, it was found that higher metal oxide concentrations lead to a slightly decreased activation energy for bulk oxygen ion transport. For CGOCo2 to CGOCo6, no difference in the activation energy for grain boundary transport was found, while for CGOFe2 to CGOFe6 the increase of Fe concentration leads to an increase of $E_{A,gb}$. The significant influence on the activation energy of the grain boundary transport is a further hint for the idea, that the added metal oxides are mainly segregated at the grain boundaries. For Cu and Co addition, an additional effect on the bulk can be deduced, which is less pronounced for Fe addition.

For V, no effect on the bulk activation energy but a slight increase of the grain boundary activation energy was found. Mn addition led to an increase of $E_{A,gb}$ and $E_{A,bulk}$.

In comparison to the literature values shown in Table IV, it can be seen, that the activation energies are mainly affected by the concentration of the main acceptor dopant. The values measured here for CGOFe2, CGOCo2, and CGOCu2, are well comparable to literature values found for similar compositions. Nevertheless, also the synthesis

Table IV. Activation energies calculated from Arrhenius diagrams of impedance spectroscopy results and comparison to literature values.

Composition	$E_{A,bulk}$/eV	$E_{A,gb}$/eV	$E_{A,total}$/eV
$Ce_{0.9}Gd_{0.1}O_{1.95}$ (CGO)	1.02 ± 0.03	1.02 ± 0.12	1.02 ± 0.11
$Ce_{0.9}Gd_{0.1}O_{1.95}$[24]	1.26 ± 0.10	1.45 ± 0.23	1.42 ± 0.21
$Ce_{0.9}Gd_{0.1}O_{1.95}$[31]	0.78 ± 0.01	0.96 ± 0.03	-
$Ce_{0.9}Gd_{0.1}O_{1.95}$[73]	-	-	0.72
$Ce_{0.8}Gd_{0.2}O_{1.9}$[33]	-	-	0.99
$Ce_{0.8}Gd_{0.2}O_{1.9}$[74]	0.81	1.30	0.88
$Ce_{0.8}Gd_{0.2}O_{1.9}$[32]	0.75 ± 0.01	-	-
$Ce_{0.99}Gd_{0.01}O_{2-\delta}$[30]	0.64	1.41 ± 0.07	-
$V_{0.04}Ce_{0.9}Gd_{0.1}O_{2-\delta}$ (CGOV4)	1.02 ± 0.04	1.27 ± 0.05	1.26 ± 0.05
$Mn_{0.02}Ce_{0.9}Gd_{0.1}O_{2-\delta}$ (CGOMn2)	1.13 ± 0.04	1.29 ± 0.11	1.27 ± 0.10
$Mn_{0.02}Ce_{0.9}Gd_{0.1}O_{2-\delta}$[24]	1.51 ± 0.20	1.47 ± 0.08	1.47 ± 0.08
$Mn_{0.005}Ce_{0.985}Gd_{0.01}O_{2-\delta}$[30]	0.65	1.35 ± 0.03	-
$Mn_{0.01}Ce_{0.79}Gd_{0.2}O_{2-\delta}$[39]	0.86	1.03	1.01
$Fe_{0.06}Ce_{0.9}Gd_{0.1}O_{2-\delta}$ (CGOFe6)	0.86 ± 0.05	1.34 ± 0.03	1.33 ± 0.03
$Fe_{0.04}Ce_{0.9}Gd_{0.1}O_{2-\delta}$ (CGOFe4)	0.88 ± 0.05	1.46 ± 0.03	1.42 ± 0.02
$Fe_{0.02}Ce_{0.9}Gd_{0.1}O_{2-\delta}$ (CGOFe2)	0.99 ± 0.08	1.19 ± 0.09	1.19 ± 0.09
$Fe_{0.005}Ce_{0.985}Gd_{0.01}O_{2-\delta}$[30]	0.64	1.23 ± 0.03	-
$Fe_{0.02}Ce_{0.97}Gd_{0.01}O_{2-\delta}$[30]	0.65	1.45 ± 0.17	-
$Fe_{0.01}Ce_{0.8}Gd_{0.2}O_{2-\delta}$[33]	-	-	0.85
$Fe_{0.02}Ce_{0.8}Gd_{0.2}O_{2-\delta}$[32]	0.81 ± 0.01	-	-
$Co_{0.06}Ce_{0.9}Gd_{0.1}O_{2-\delta}$ (CGOCo6)	0.75 ± 0.04	1.23 ± 0.10	1.20 ± 0.09
$Co_{0.04}Ce_{0.9}Gd_{0.1}O_{2-\delta}$ (CGOCo4)	0.91 ± 0.06	1.25 ± 0.08	1.20 ± 0.07
$Co_{0.02}Ce_{0.9}Gd_{0.1}O_{2-\delta}$ (CGOCo2)	0.90 ± 0.02	1.22 ± 0.08	1.19 ± 0.07
$Co_{0.02}Ce_{0.8}Gd_{0.2}O_{2-\delta}$[32]	0.82 ± 0.01	-	-
$Co_{0.01}Ce_{0.8}Gd_{0.2}O_{2-\delta}$[33]	-	-	0.63
$Co_{0.02}Ce_{0.9}Gd_{0.1}O_{2-\delta}$[31]	0.70 ± 0.02	0.91 ± 0.01	-
$Co_{0.005}Ce_{0.985}Gd_{0.01}O_{2-\delta}$[30]	0.64	1.01 ± 0.03	-
$Cu_{0.02}Ce_{0.9}Gd_{0.1}O_{2-\delta}$ (CGOCu2)	0.90 ± 0.03	1.13 ± 0.11	1.13 ± 0.11
$Cu_{0.02}Ce_{0.8}Gd_{0.2}O_{2-\delta}$[32]	0.85 ± 0.01	-	-
$Cu_{0.005}Ce_{0.985}Gd_{0.01}O_{2-\delta}$[30]	0.64	1.32 ± 0.02	-

of the samples plays an important role for the transport characteristics. A difference between our values and the values from other publications may arise because transition metal cation doped ceria is often produced from the respective nitrates by precipitation and subsequent calcination and not by mixed oxide synthesis. Effects of synthesis and related effects of grain/grain boundary ratio (grain size of the different samples) may also explain significant differences between the activation energies for Gd-doped ceria from various publications (cf. Table IV).

Microcontact Hebb-Wagner measurements.—The graphs for the Co containing samples in Fig. 8 show a striking deviation from the normal V-shape of the oxygen partial pressure dependence of the electronic conductivity: in the partial pressure range between 10^{-4} and 10^{-8} bar, there is even a maximum of the electronic conductivity, in particular between 700 to 500°C. This maximum was always found for microcontact polarization from −0.8 to 0 V but not in the reverse direction. When averaging the values, the standard deviation in this area is therefore quite high (cf. Fig. 9). This behavior was already observed, but not discussed in an earlier publication.[31] An increase of the hole conductivity with decreasing oxygen partial pressure strongly hints at an oxidation from Co^{2+} back to Co^{3+}. The effect is possibly only observable in one measurement direction as the reduction of Co^{3+} is slower than the polarization time used in the experiment and therefore does not resolve as a single peak.

For the other compositions such a maximum has not been observed, although V as well as Mn or Fe are known to exist in several oxidation states. This either means, that these cations already exist in their lowest oxidation state within the material, or that the reduction/oxidation process is not resolved in the measurements, because it takes longer than the polarization time or is smeared over a broader partial pressure range.

Regarding the intermediate oxygen partial pressure range from room air to 10^{-10} bar in Fig. 10, it can be observed that the electron conductivity of the pristine CGO and CGOFe4, CGOV4 and CGOMn2 at 800°C is very similar, while CGOCu2 and CGOCo6 show a slightly enhanced electron conductivity at this temperature. It can be seen that 2 cat% Cu addition has a similarly strong effect on the electronic conductivity as 6 cat% Co addition. Interestingly, CGOCo6 and CGOCu2 also show a slight shift of the electronic conductivity minimum to lower oxygen partial pressures. This means that a p-type conduction is favored. Fagg et al. report a slightly increased p-type conductivity for 2 cat% Fe, Co and Cu doping in $Ce_{0.8}Gd_{0.2}O_{2-\delta}$ in the oxygen partial pressure range between 0.21 bar and 10^{-4} bar.[32] Also, for Fe doping, a slight increase of the n- and p-type conductivity can be observed in our case, while the position of the minimum is not shifted compared to pure CGO. This is in accordance to the idea, that Fe addition introduces an additional state between the top of the valence band and the bottom of the Ce 4f band.[47]

In contrast, in the very low oxygen partial pressure range below 10^{-12} bar, CGOFe2 exhibits the highest electron conductivity of all materials at 800°C and CGOCo6 shows the lowest conductivity. This is in good accordance to the idea that the grain boundaries in CGOFe2 show a high potential barrier at high temperature regime, which on the one hand hinders ionic transport but on the other hand improves electron transport along the grain boundaries.

Comparing the activation energies for hole and electron transport (cf. Table V), it can be seen that V and Mn addition leads to similar or slightly decreased values for the electron transport while $E_{A,e}$ is moderately increased for addition of Fe, Co, and Cu. For CGOCo6 the strongest reduction of both activation energies can be found.

Comparison.—Combining the findings from impedance spectroscopy and Hebb-Wagner measurements, the effect of the five investigated transition metals can be categorized according to their influence on the total conductivity and electronic partial conductivity. In order to facilitate this comparison, ionic transference numbers (cf. Table VI) have been calculated from the quotient of the electronic

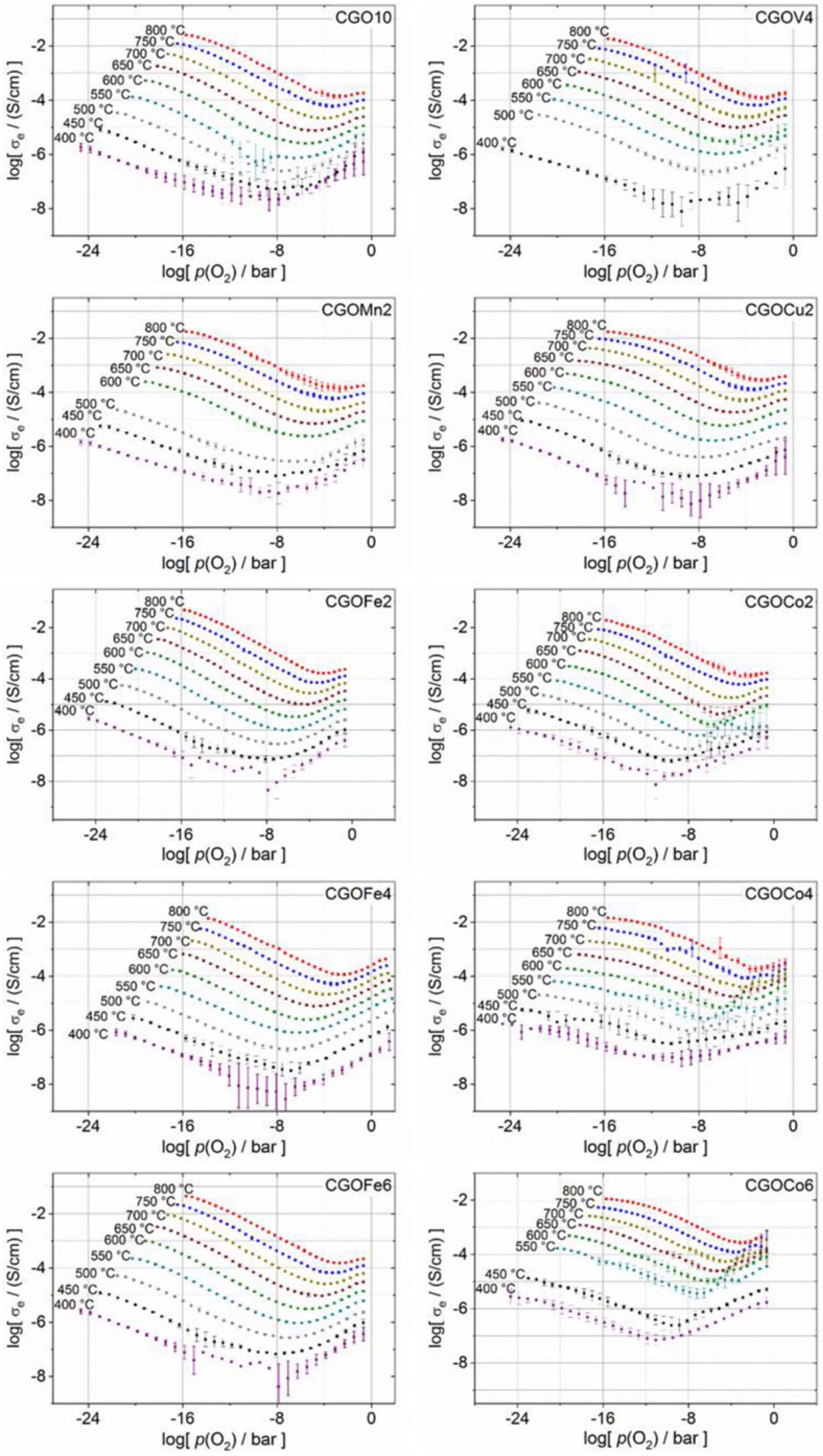

Figure 8. Average electron conductivity at variable oxygen partial pressure and temperature calculated from Hebb-Wagner current-voltage measurements for the samples with 2 mol% oxide addition. All values are corrected for the microcontact diameter but not for contact resistance and therefore represent a worst-case estimate of the electron conductivity. Error bars show standard deviation of forward and backward polarization experiments.

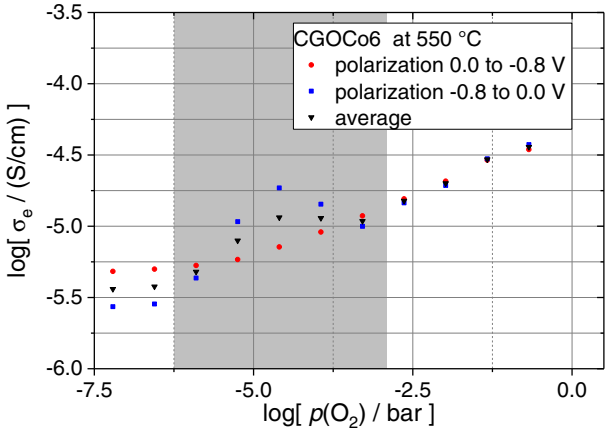

Figure 9. Forward and backward polarization of one experiment for CGOCo6 sample at 550°C. The oxygen partial pressure range, which shows indication for $Co^{3+/2+}$ redox reaction, is highlighted in gray.

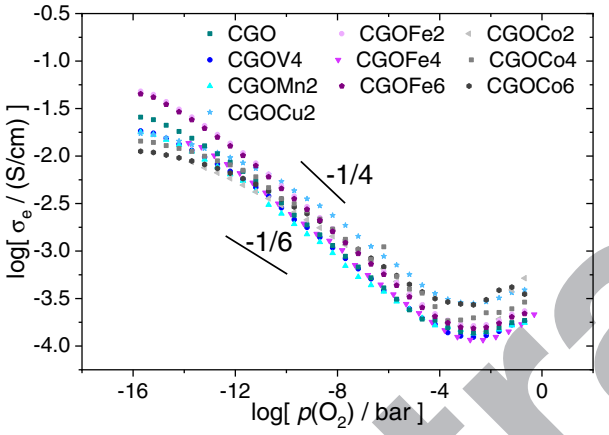

Figure 10. Comparison of the electron conductivity of all samples at 800°C.

conductivity at 0.21 bar oxygen partial pressure and from impedance spectroscopy measurements at 500–700°C ($t_{O^{2-}} = \frac{\sigma_{tot}-\sigma_e}{\sigma_{total}}$). For $\sigma_e \approx \sigma_{total}$ values near zero are received. This is the case for pure CGO and CGOCo4 at 500°C and CGOCo6 at 600°C.

Comparing the ionic transference numbers at 700°C (cf. Table VI), CGOCo6 shows the lowest one of all measured samples with a value of 0.23. CGOCo2, on the other hand, together with CGOFe4 and CGOFe6, shows the highest ionic transference numbers even at low

Table V. Activation energies for p-type ($E_{A,h}$) and n-type transport ($E_{A,e}$) derived from the average results of conductivity measurements at $pO_2 = 0.21$ bar and $pO_2 = 10^{-10}$ bar, respectively. Literature values for 20 cat% Gd doped ceria are shown for comparison.

Composition	$E_{A,h}$	$E_{A,e}$
CGO	0.99 ± 0.04	1.97 ± 0.13
$Ce_{0.8}Gd_{0.2}O_{1.9}$[74]	1.16 ± 0.04	2.59 ± 0.07
CGOV4	1.10 ± 0.05	1.80 ± 0.12
CGOMn2	1.16 ± 0.16	1.86 ± 0.10
CGOFe6	1.04 ± 0.03	1.74 ± 0.08
CGOFe4	1.12 ± 0.01	2.07 ± 0.05
CGOFe2	1.15 ± 0.01	2.07 ± 0.05
CGOCo6	0.88 ± 0.05	1.76 ± 0.05
CGOCo4	1.08 ± 0.02	2.00 ± 0.10
CGOCo2	1.03 ± 0.10	2.18 ± 0.07
CGOCu2	1.22 ± 0.05	2.10 ± 0.07

Table VI. Ionic transference number calculated from total conductivities from impedance spectroscopy measurements and the electron partial conductivity at oxygen partial pressure of air from Hebb-Wagner measurements at selected temperatures. The error for the transference numbers is estimated to be in the range of 10% due to the combined errors of electronic and electrical conductivity measurement. Literature values are shown for comparison.

Composition	$t_{O^{2-}}$ 500°C	600°C	700°C
CGO	0.00	0.79	0.90
$Ce_{0.8}Gd_{0.2}O_{1.9}$[74]	-	0.99	-
CGOV4	0.18	0.61	0.65
CGOMn2	0.47	0.82	0.92
$Mn_{0.02}Ce_{0.9}Gd_{0.1}O_{1.95}$[24]	-	0.61	0.86
CGOFe6	0.69	0.83	0.87
CGOFe4	0.77	0.88	0.92
CGOFe2	0.47	0.79	0.85
$Fe_{0.02}Ce_{0.8}Gd_{0.2}O_{1.9}$[32]	-	-	0.98
CGOCo6	0.00	0.00	0.23
CGOCo4	0.00	0.07	0.54
CGOCo2	0.69	0.84	0.92
$Co_{0.02}Ce_{0.8}Gd_{0.2}O_{1.9}$[32]	-	-	0.97
CGOCu2	0.37	0.36	0.65
$Cu_{0.02}Ce_{0.8}Gd_{0.2}O_{1.9}$[32]	-	-	0.97

temperatures. CGOFe2 and CGOMn2 have a slightly enhancing effect on the ionic transport while for CGOCu2 and CGOV4, an increase of the mixed conductivity even at high temperatures was found, as well.

For the high temperature range 600–800°C for which most of the literature studies can be found, the influence of transition metal oxides on the electrical conductivity is rather small, apart from the case of Co addition. This is in good agreement to previous findings where no changes were found for e.g. Co, Fe or Cu oxide addition,[32] but a slight decrease of electrical conductivity for addition of Mn oxide.[33,34] In contrast, a significant deviation can be seen in the temperature range 200–400°C. Here, CGOMn2, CGOCu2 and CGOCo6 show the highest increase in bulk conductivity, which is about 2.5 decades higher as compared to pure CGO (compared to CGOMn2 at 200°C). By comparing the impedance spectroscopy data of the Co- and Fe-doped samples to studies, where the transition metals were added to CGO powder as solution of the respective nitrates in ethanol, shows that the synthesis method from oxides we chose for our study is not optimal. Adding the transition metals as an ethanolic solution, which has been done in these studies,[31,53] apparently leads to a better distribution of the transition metals and increases the improvement of grain boundary conductivity for low concentrations of metal additive, which was already expected.

The published results concerning the influence on the electronic conductivity for the intensely investigated metals Co and Fe broadly fit to our findings: In our study, only a small influence on the p-type conductivity was found for 2 cat% Fe and Co doped materials as well as for Cu, with CGOCo6 and CGOCu2 exhibiting similar increases. This is comparable to findings of Fagg et al.[32] and Myung et al.[72] For the n-type range, CGOCo6 shows a significant decrease of the electron conductivity with increasing oxygen partial pressure especially in the low oxygen partial pressure range below 10^{-12} bar. Here, the addition of Fe showed the highest increase in the electron conductivity compared to all other samples.

The behavior of CGOCo6 is of special interest, as the bulk and grain boundary was severely impaired by Co addition, but the electronic conductivity of the material is strongly increased. Reproducible results for this composition were obtained with different samples from two different batches of powder. This is an indication for the development of secondary phases (presumably at the grain boundaries). If these phases do not form a percolation network (which is not to be expected at such low concentrations) and if the secondary phases show electronic conductivity but are not oxygen ion conductive, or show only an inferior ionic conductivity, an increase of the electronic

conductivity and parallel decrease of electrical conductivity should be observed. By comparing CGOFe2 to CGOFe6, in contrast, no strong effect on the bulk and grain boundary conductivity was observed, although the formation of secondary phases has already been reported.[45]

Vanadium addition to acceptor doped ceria and subsequent analysis of the electrochemical behavior was not performed before to the knowledge of the authors. A donor doping effect by V_2O_5 addition - as initially expected from comparison with Ta_2O_5 and Nb_2O_5 - could not be confirmed by the experiments. Nevertheless, further study of the effects of V addition could be interesting as a significantly lowered electrical conductivity was observed for CGOV4, especially in the low temperature regime. Together with the inhibition of grain growth in comparison to other sampled material, V addition could have similar "poisoning" effects on ceria like Cr addition.[31,35]

Conclusions and Outlook

A screening of the effect of transition metal oxide addition on the electronic conductivity and grain boundary transport characteristics of commercial CGO as comparable host material was performed with a variety of measurement methods. Apart from yielding comparable electrochemical data, the mixing of ceria and metal oxides also mimics the effect of co-sintering ceria with transition metal oxide containing components like stainless steel supports, certain perovskites or spinels, although even better results would have been received by other synthesis methods.

Our investigations mainly focused on the changes of electronic conductivity and the grain boundary transport behavior of CGO introduced by addition of transition metal oxides. The main idea was to provide a range of samples with different compositions, which underwent the same synthesis procedure in order to get better comparability of the effect of the additives. Measurements of the electronic conductivities within such a large continuous oxygen partial pressure and temperature range have not been published for these materials, yet. As the electronic conductivity is mostly the rate determining step for oxygen transport through ceria-based membranes, an exact knowledge of the electronic transport processes is crucial for optimization of the materials.

Summing up our findings for the effect of transition metal oxide addition, the main conclusion was that even small amounts of transition metal oxides have a vast effect especially on the electronic charge carrier transport. The role of the transition metal oxides becomes even more pronounced at temperatures $\lesssim 500°C$, making them especially interesting in the area of low temperature applications in industry. The comprehensive data on the effects on the electronic and grain boundary transport characteristics compiled in this study will ameliorate the prediction of the effect of interdiffusion of metal cations in complex ceria based systems. In the future, the effect of different transition metal cations could possibly be exploited to improve the performance of ceria-based materials by deliberately choosing metal oxide sintering aids depending on whether the cerium dioxide compound needs to have a high oxygen ion conductivity or a high mixed conductivity. For high oxygen ion conductivity, Fe and Mn oxide addition is beneficial, as well as the addition of small amounts of Co oxide, while V and Cu oxide addition support high mixed conductivity.

Further investigations will address the respective effects of the transition metal concentrations especially for transition metal cations with different valences. The interesting redox-activity related increase of the electronic conductivity found for the Co doped samples deserves a detailed analysis.

Acknowledgments

The authors thank Daniel Borecki, Jan-Paul Brinkmann, Nils Klöcker and Jan Sietman who prepared and measured part of the samples during their internship. The research for this article was funded by the German Research Foundation (DFG), project #387282673.

ORCID

Kerstin Neuhaus https://orcid.org/0000-0002-3519-3987
Raimund Dolle https://orcid.org/0000-0001-6777-8421
Hans-Dieter Wiemhöfer https://orcid.org/0000-0002-6049-9953

References

1. H. Takamura, T. Kobayashi, T. Kasahara, A. Kamegawa, and M. Okada, *J Alloys Compd*, **408–412**, 1084 (2006).
2. H. Takamura, Y. Koshino, A. Kamegawa, and M. Okada, *Solid State Ionics*, **177**(19–25), 2185 (2006).
3. H. Takamura, K. Okumura, Y. Koshino, A. Kamegawa, and M. Okada, *J Electroceram*, **13**(1), 613 (2004).
4. M. Ramasamy, S. Baumann, J. Palisaitis, F. Schulze-Küppers, M. Balaguer, D. Kim, W. A. Meulenberg, J. Mayer, R. Bhave, and O. Guillon, *J Am Ceram Soc*, **99**(1), 349 (2016).
5. M. Balaguer, J. García-Fayos, C. Solís, and J. M. Serra, *Chem Mater*, **25**(24), 4986 (2013).
6. V. V. Kharton, A. V. Kovalevsky, A. P. Viskup, F. M. Figueiredo, A. A. Yaremchenko, E. N. Naumovich, and F. M. B. Marques, *J Electrochem Soc*, **147**(7), 2814 (2000).
7. V. V. Kharton, A. V. Kovalevsky, A. P. Viskup, A. L. Shaula, F. M. Figueiredo, E. N. Naumovich, and F. M. B. Marques, *Solid State Ionics*, **160**(3), 247 (2003).
8. K. Wang, R. Ran, W. Zhou, H. Gu, Z. Shao, and J. Ahn, *J Pow Source*, **179**(1), 60 (2008).
9. N. Shaigan, W. Qu, D. G. Ivey, and W. Chen, *J Pow Source*, **195**(6), 1529 (2010).
10. D. Terribile, A. Trovarelli, C. de Leitenburg, A. Primavera, and G. Dolcetti, *Catal Tod*, **47**(1–4). 133 (1999).
11. R. Dziembaj, M. Molenda, L. Chmielarz, M. Drozdek, M. M. Zaitz, B. Dudek, A. Rafalska-Łasocha, and Z. Piwowarska, *Catal lett*, **135**(1-2), 68 (2010).
12. M. Martinez-Huerta, J. Coronado, M. Fernandez-Garcia, A. Iglesias-Juez, G. Deo, J. Fierro, and M. Banares, *J Catal*, **225**(1), 240 (2004).
13. E. Aneggi, M. Boaro, C. de Leitenburg, G. Dolcetti, and A. Trovarelli, *J. Alloy Compd.*, **408–412**(0), 1096 (2006).
14. O. H. Laguna, M. A. Centeno, G. Arzamendi, L. M. Gandía, F. Romero-Sarria, and J. A. Odriozola, *Catalysis Today*, **157**(1), 155 (2010).
15. F. J. Perez-Alonso, I. Melián-Cabrera, M. López Granados, F. Kapteijn, and J. L. G. Fierro, *Journal of Catalysis*, **239**(2), 340 (2006).
16. A. Maheshwari, M. Daniels, K. Schmale, and H.-D. Wiemhöfer, *International Proceedings of Computer Science and Information Technology*, **56**, 85 (2012).
17. M. C. Göbel, G. Gregori, and J. Maier, *Solid State Ionics*, **215**, 45 (2012).
18. M. R. De Guire, M. J. Shingler, and E. Dincer, *Solid State Ionics*, **52**(1–3), 155 (1992).
19. Y. Xiong, K. Yamaji, T. Horita, N. Sakai, and H. Yokokawa, *J. Electrochem. Soc.*, **151**(3), A407 (2004).
20. M. B. Mogensen, N. M. Sammes, and G. A. Tompsett, *Solid State Ionics*, **129**, 63 (2000).
21. D. L. Maricle, D. E. Swarr, and S. Karavolis, *Solid State Ionics*, **52**(1-3), 173 (1992).
22. J. A. Kilner, *Chem Lett*, **37**(10), 1012 (2008).
23. S. R. Bishop, T. S. Stefanik, and H. L. Tuller, *Phys Chem Chem Phys*, **13**(21), 10165 (2011).
24. K. Neuhaus, S. Baumann, R. Dolle, and H.-D. Wiemhöfer, *Crystals*, **8**(1), (2018).
25. K. Schmale, M. Grünebaum, M. Janssen, S. Baumann, F. Schulze-Küppers, and H.-D. Wiemhöfer, *Physica Status Solidi B*, **248**(2), 314 (2011).
26. K. Neuhaus, S. Eickholt, A. Maheshwari, F. Schulze-Küppers, S. Baumann, and H.-D. Wiemhöfer, *J Electrochem Soc*, **164**(7), H491 (2017).
27. K. Sasaki and J. Maier, *Phys Chem Chem Phys*, **2**(13), 3055 (2000).
28. Z. Tianshu, P. Hing, H. Huang, and J. Kilner, *Mat Sci Eng B*, **83**(1), 235 (2001).
29. W. Cen, Y. Liu, Z. Wu, H. Wang, and X. Weng, *Phys Chem Chem Phys*, **14**(16), 5769 (2012).
30. H. J. Avila-Paredes and S. Kim, *Solid State Ionics*, **177**(35–36), 3075 (2006).
31. S. Taub, K. Neuhaus, H.-D. Wiemhöfer, N. Ni, J. A. Kilner, and A. Atkinson, *Solid State Ionics*, **282**, 54 (2015).
32. D. P. Fagg, V. V. Kharton, and J. R. Frade, *J Electroceram*, **9**(3), 199 (2002).
33. E. Y. Pikalova, A. N. Demina, A. K. Demin, A. A. Murashkina, V. E. Sopernikov, and N. O. Esina, *Inorg Mater*, **43**(7), 735 (2007).
34. S.-H. Park and H.-I. Yoo, *Solid State Ionics*, **176**(15–16), 1485 (2005).
35. S. Taub, R. E. A. Williams, X. Wang, D. W. McComb, J. A. Kilner, and A. Atkinson, *Acta Materialia*, **81**, 128 (2014).
36. G. Hua, X. Ding, W. Zhu, and J. Li, *J Mater Sci - Mater El*, **26**(6), 3664 (2015).
37. T. Zhang, P. Hing, H. Huang, and J. A. Kilner, *J Mat Proc Tech*, **113**(1), 463 (2001).
38. C. R. Foschini, D. P. F. Souza, P. I. Paulin Filho, and J. A. Varela, *J Euro Ceram Soc*, **21**(9), 1143 (2001).
39. T. Zhang, L. Kong, Z. Zeng, H. Huang, P. Hing, Z. Xia, and J. Kilner, *J Sol State Electrochem*, **7**(6), 348 (2003).
40. K. Schmale, M. Daniels, A. Buchheit, M. Grünebaum, L. Haase, S. Koops, and H.-D. Wiemhöfer, *J. Electrochem. Soc.*, **160**(9), F1081 (2013).
41. S. Li, L. Ge, H. Gu, Y. Zheng, H. Chen, and L. Guo, *Journal of Alloys and Compounds*, **509**(1), 94 (2011).
42. C. M. Kleinlogel and L. J. Gauckler, *J. Electroceram.*, **5**(3), 231 (2000).
43. E. Jud and L. J. Gauckler, *J. Electroceram.*, **15**, 159 (2005).
44. W. Zajac, L. Suescun, K. Świerczek, and J. Molenda, *J Pow Source*, **194**(1), 2 (2009).
45. E. V. Tsipis, J. C. Waerenborgh, and V. V. Kharton, *J Solid State Electrochem*, **21**, 2965 (2017).

46. X. Guo and R. Waser, *Prog. Mater. Sci.*, **51**(2), 151 (2006).
47. A. Khare, R. J. Choudhary, D. M. Phase, and S. P. Sanyal, *J Appl Phys*, **109**(12), 123706 (2011).
48. K. N. Rao, B. M. Reddy, B. Abhishek, Y.-H. Seo, N. Jiang, and S.-E. Park, *Appl Catal B*, **91**(3), 649 (2009).
49. D. Li, J. Yu, M. Chao, M. Li, H. Wu, and E. Liang, *Ionics*, **19**(9), 1291 (2013).
50. R. Li, S. Yabe, M. Yamashita, S. Momose, S. Yoshida, S. Yin, and T. Sato, *Mater Chem Phys*, **75**(1), 39 (2002).
51. L. Gao, M. Zhou, Y. Zheng, H. Gu, H. Chen, and L. Guo, *J Pow Source*, **195**(10), 3130 (2010).
52. C. Y. Kang, H. Kusaba, H. Yahiro, K. Sasaki, and Y. Teraoka, *Solid State Ionics*, **177**(19–25), 1799 (2006).
53. R. R. Kondakindi and K. Karan, *Mat Chem Phys*, **115**(2–3), 728 (2009).
54. C. Zhang, J. Sunarso, Z. Zhu, S. Wang, and S. Liu, *Solid State Ionics*, **310**, 121 (2017).
55. M. Hrovat, J. Holc, S. Bernik, and D. Makovec, *Materials Research Bulletin*, **33**(8), 1175 (1998).
56. J. C. Wurst and J. A. Nelson, *J Am Ceram Soc*, **55**(2), 109 (1972).
57. K. Schmale, M. Daniels, A. Buchheit, M. Grünebaum, L. Haase, S. Koops, and H.-D. Wiemhöfer, *J Electrochem Soc*, **160**(9), F1081 (2013).
58. A. Jasper, J. A. Kilner, and D. W. McComb, *Solid State Ionics*, **179**(21), 904 (2008).
59. J.-H. Hwang, D. S. McLachlan, and T. O. Mason, *J Electroceram*, **3**(1), 7 (1999).
60. J. Fleig, *Solid State Ionics*, **150**(1), 181 (2002).
61. S. M. Haile, D. L. West, and J. Campbell, *J Mater Res*, **13**(6), 1576 (2011).
62. G. M. Christie and F. P. F. Van Berkel, *Solid State Ionics*, **83**(1), 17 (1996).
63. J.-P. Eufinger, M. Daniels, K. Schmale, S. Berendts, G. Ulbrich, M. Lerch, H.-D. Wiemhöfer, and J. Janek, *Phys Chem Chem Phys*, **16**(46), 25583 (2014).
64. K. Schmale, M. Grünebaum, M. Janssen, S. Baumann, F. Schulze-Küppers, and H.-D. Wiemhöfer, *Phys Stat Sol B*, **248**(2), 314 (2011).
65. S. Lübke and H.-D. Wiemhöfer, *Solid State Ionics*, **117**(3–4), 229 (1999).
66. K. Biswas, *Ceram Inter*, **35**(4), 1521 (2009).
67. S. Kim and J. Maier, *J Electrochem Soc*, **149**(10), J73 (2002).
68. R. Waser and R. Hagenbeck, *Acta Materialia*, **48**(4), 797 (2000).
69. X. Guo, W. Sigle, and J. Maier, *J. Am. Ceram. Soc.*, **86**(1), 77 (2003).
70. B. Wang and Z. Lin, *International Journal of Hydrogen Energy*, **39**(26), 14334 (2014).
71. A. Tschöpe, S. Kilassonia, and R. Birringer, *Solid State Ionics*, **173**(1), 57 (2004).
72. J. Myung, T. H. Shin, X. Huang, G. Carins, and J. T. S. Irvine, *Int. J. Hydrogen. En.*, **40**(35), 12003 (2015).
73. J. Faber, C. Geoffroy, A. Roux, A. Sylvestre, and P. Abélard, *Appl Phys A*, **49**(3), 225 (1989).
74. S. Lübke and H.-D. Wiemhöfer, *Solid State Ionics*, **117**, 229 (1999).